World Scientific
www.worldscientific.com

A POSTERIORI TESTS OF ONE-EQUATION LES MODELING OF ROTATING TURBULENCE

HAO LU* and CHRISTOPHER J. RUTLAND†

Mechanical Engineering, University of Wisconsin-Madison
1500 Engineering Drive, Madison, WI 53706, USA
*haolu630@gmail.com
†luxxx347@umn.edu

LESLIE M. SMITH

Mathematics and Engineering Physics
University of Wisconsin-Madison
480 Lincoln Drive, Madison, WI 53706, USA
lsmith@math.wisc.edu

Eight subgrid-scale (SGS) models were evaluated using two flow configurations: homogeneous decaying turbulence, and rotating turbulence forced at large or intermediate scales. Testing was performed for the first configuration through a systematic comparison between direct numerical simulation results and large eddy simulation results of many characteristics, including resolved kinetic energy, SGS energy production, molecular dissipation, and kinetic energy spectrum. The new models, which are based on dynamic structure model and satisfy the consistency of material frame indifference with the SGS stress, showed more accurate results than traditional models. In the forced testing, the new models were better able to capture essential features of rotating turbulence, including cyclonic/anti-cyclonic asymmetry, quasi-2D at large scales, and reverse kinetic energy transfer from small to large scales.

Keywords: Rotating turbulence; large eddy simulation; dynamic structure model.

1. Introduction

Rotation has a significant influence on large-scale atmospheric and oceanic flows as well as some engineering flows (e.g., turbulence in jet engines). The Coriolis force appears in the momentum equations as a linear part; however, it may radically change the nonlinear dynamics. Studies, including experiments, theoretical analysis, and numerical simulations, have addressed that rotation turbulence has many characteristic features, such as the tendency toward 2D flow,[7,2] the cyclonic/anti-cyclonic asymmetry in favor of cyclone,[36,30] and the influence of the background rotation on the kinetic energy transfer, including the reduced transfer from large

scales to small scales and the reverse transfer from small scales to large scales.[7,28] To deliver these features, accurate modeling of the effects of rotation on turbulence using large eddy simulation (LES) is a great challenge.

The LES equations of homogeneous incompressible rotating flow are

$$\frac{\partial \bar{u}_i}{\partial x_i} = 0\,, \quad \frac{\partial \bar{u}_i}{\partial t} + \frac{\partial \bar{u}_i \bar{u}_j}{\partial x_j} = -\frac{\partial \bar{p}}{\partial x_i} - 2\Omega \epsilon_{i3j} \bar{u}_j + \nu \frac{\partial^2 \bar{u}_i}{\partial x_j \partial x_j} + \bar{f}_i - \frac{\partial \tau_{ij}}{\partial x_j}\,, \quad (1)$$

where $\bar{p}$ is the effective pressure, ν is the kinematic viscosity, $\bar{f}_i$ is a forcing term, Ω is the (constant) rotation rate, and the subgrid-scale (SGS) stress tensor is $\tau_{ij} = \overline{u_i u_j} - \bar{u}_i \bar{u}_j$. The goal of LES modeling is to represent the SGS stress in terms of the resolved velocity field, $\bar{u}_i(\mathbf{x}, t)$. Most traditional turbulent models are based on the assumption that small-scale turbulence is isotropic, and they may perform poorly in the presence of rotation.

Speziale[38] and Fureby and Tabor[14] carried out analyses of the frame transformation properties of the SGS stress. Further, studies have stated that the consistency of material frame indifference (MFI) should be imposed not only on the vector level $\partial \tau_{ij}/\partial x_j$ but also on the tensor level τ_{ij} itself,[34,21,18,25] and most of the existing SGS models are not MFI consistent. It can be guaranteed that "the implementation of the correction terms into the SGS models in actual LES yields results no different from those obtained without implementation of the correction terms," only if the SGS models obey the same transformation rules as the exact SGS stress tensor.[18] In other words, LES in a rotating frame using an MFI consistent model can avoid the error that results from frame transformation.[25]

The goal of the current research is to perform a comparative study of LES using various SGS models. This work follows our previous *a priori* study[25] of LES models in rotating turbulence. We test the following traditional SGS models, which are important representatives of the available SGS models: the Smagorinsky model,[35] the dynamic Smagorinsky model (DynSM),[15,23] the scale similarity model,[1,24] the mixed scale similarity model (MSSM),[42,39] the subgrid kinetic energy model (KEM),[12,16,20,27] and the dynamic structure model (DSM).[33,10] We also assess two new mixed one-equation models that are in the DSM family and are developed based on the assumption that the modeled stress tensor is MFI consistent.[25]

The remainder of this paper is organized as follows. Section 2 reviews SGS models and presents the development of new models. Section 3 compares LES results with filtered DNS data for decaying turbulence. The results of forced rotating turbulent flows are discussed in Sec. 4, and Sec. 5 summarizes the findings.

2. SGS Models and Numerical Methods

2.1. *Traditional SGS models*

Based on the Boussinesq hypothesis,[6] a common class of SGS models describes the trace-free part of the SGS tensor using the form $\tau_{ij} - (\tau_{kk}/3)\delta_{ij} \approx -2\nu_t \bar{S}_{ij}$,

where $\bar{S}_{ij} = (1/2)(\partial \bar{u}_i/\partial x_j + \partial \bar{u}_j/\partial x_i)$ and ν_t is the eddy viscosity. Smagorinsky[35] introduced the first expression, $\nu_t = (C_s \Delta)^2 |\bar{S}|$, where $|\bar{S}| = (2\bar{S}_{ij}\bar{S}_{ij})^{1/2}$, and we adopt the Smagorinsky coefficient, $C_s = 0.18$, in the paper as suggested by Lilly.[22] This model is denoted as SM for subsequent discussions.

However, for complex flows, it may not be possible to find a single universal constant that is appropriate for the entire domain at all times. Thus, Germano *et al.*[15] and Lilly[23] proposed the DynSM, $\nu_t = C_D(\Delta)^2 |\bar{S}|$. The Germano identity[15] defines a test filtering whose width $\hat{\Delta}$ is larger than the grid filter width Δ (typically $\hat{\Delta} = 2\Delta$). Using the least-square-error approach, the model coefficient is determined as $C_D = (\langle L_{ij} M_{ij}\rangle / \langle M_{kl} M_{kl}\rangle)$, where $\langle \cdot \rangle$ represents the arithmetic mean, $L_{ij} = \widehat{\bar{u}_i \bar{u}_j} - \hat{\bar{u}}_i \hat{\bar{u}}_j$ and $M_{ij} = 2(\Delta^2 \widehat{|\bar{S}|\bar{S}_{ij}} - \hat{\Delta}^2 |\hat{\bar{S}}|\hat{\bar{S}}_{ij})$.

The KEM is another widely used eddy viscosity model,[12,16,20,27] by which the full SGS stress is modeled as $\tau_{ij} \approx (2/3)k_{\text{sgs}}\delta_{ij} - 2\nu_k \bar{S}_{ij}$, where $k_{\text{sgs}} = (1/2)\tau_{kk}$ and $\nu_k = C_k \sqrt{k_{\text{sgs}}}\Delta$. An approximation for k_{sgs} is obtained solving the transport equation

$$\frac{\partial k_{\text{sgs}}}{\partial t} + \bar{u}_j \frac{\partial k_{\text{sgs}}}{\partial x_j} = -\tau_{ij}\frac{\partial \bar{u}_i}{\partial x_j} - C_c \frac{k_{\text{sgs}}^{3/2}}{\Delta} + \frac{\partial}{\partial x_j}\left[\left(\frac{\nu_k}{\sigma_k} + \nu\right)\frac{\partial k_{\text{sgs}}}{\partial x_j}\right]. \qquad (2)$$

Here, the three terms on the right-hand side represent, respectively, the production, the dissipation, and the diffusion. The constants are typically chosen as $C_k = 0.05$, $C_c = 1.0$, and $\sigma_k = 1.0$ based on a previous study by Yoshizawa and Horiuti.[41]

The eddy viscosity closure assumes a one-to-one correlation between τ_{ij} and $\bar{S}_{ij}$. However, studies using DNS data[11,27,25] and experimental data[24] have displayed very little correlation between them. Thus, Bardina *et al.*[1] proposed the original scale similarity model in 1980. We study a modified version whose expression is Galilean invariant, $\tau_{ij} \approx C_L L_{ij}^M$, where $L_{ij}^M = \overline{\bar{u}_i \bar{u}_j} - \bar{\bar{u}}_i \bar{\bar{u}}_j$, and we set $C_L = 1.0$ in this paper. This model is denoted as SSM for subsequent discussions.

Bardina *et al.*[1] have also noted that the scale similarity model alone is not dissipative enough and causes numerical instability, and thus introduced a linear combination of this model and an eddy viscosity model. Zang *et al.*[42] proposed a dynamic mixed approach to calculate the eddy viscosity model coefficient. Vreman *et al.*[39] introduced an improvement version removing some mathematical inconsistencies. The MSSM is written as $\tau_{ij} \approx C_L L_{ij}^M - 2C_D^{\text{SSM}}\Delta^2 |\bar{S}|\bar{S}_{ij}$, where $C_D^{\text{SSM}} = (\langle (L_{ij} - H_{ij}) M_{ij}\rangle / \langle M_{kl} M_{kl}\rangle)$ and $H_{ij} = \widehat{\hat{\bar{u}}_i \hat{\bar{u}}_j} - \hat{\hat{\bar{u}}}_i \hat{\hat{\bar{u}}}_j - (\widehat{\overline{\bar{u}_i \bar{u}_j}} - \widehat{\bar{u}_i \bar{u}_j})$.

Pomraning and Rutland[33] introduced the DSM. Although it is a nonviscosity model, it yields good agreement with filtered DNS data at the *a posteriori* test level for low-Reynolds number isotropic turbulence.[10] This model uses a tensor form of the SGS stresses: $\tau_{ij} = C_{ij}k_{\text{sgs}}$. Note that C_{ij} must satisfy $C_{ii} = 2$. Assuming the same form at the test filtering level, $T_{ij} = \widehat{\bar{u}_i \bar{u}_j} - \hat{\bar{u}}_i \hat{\bar{u}}_j = C_{ij}K$, and integrating it into the Germano identity, one finds $T_{ij} - \hat{\tau}_{ij} = \widehat{\bar{u}_i \bar{u}_j} - \hat{\bar{u}}_i \hat{\bar{u}}_j = C_{ij}K - \widehat{C_{ij}k_{\text{sgs}}} \approx C_{ij}(K - \widehat{k_{\text{sgs}}})$. For this model, the structure of τ_{ij} is extracted from L_{ij}, and k_{sgs} helps predict the magnitude. For equal test and grid filter sizes, this model reduces

to an algebraic expression, $\tau_{ij} \approx (L_{ij}^M/L_{mm}^M)2k_{\text{sgs}}$. This model is a one-equation model and needs the transport equation (2) for k_{sgs}.

2.2. *Mixed MFI consistent DSMs*

At the *a priori* test level, the DSM has been shown to have excellent agreement with the actual SGS stresses in isotropic turbulence.[25] However, the modeled stress tensor is not MFI consistent with the exact SGS stress tensor. Studies[18,25] have stated that the nonlinear model and the summation of the modified Leonard term and the modified cross term, $L_{ij}^M + C_{ij}^M$, where $C_{ij}^M = \overline{\bar{u}_i u_j'} + \overline{u_i' \bar{u}_j} - \bar{u}_i \overline{u_j'} - \overline{u_i'} \bar{u}_j$, are MFI consistent. Thus, in previous work we proposed two models in the DSM family that are MFI consistent.[25]

To provide adequate dissipation at small scales, we include an eddy viscosity term. Further, to overcome the weakness that the traditional eddy viscosity $(-2\nu_t \bar{S}_{ij})$ is too dissipative at large scales, which may hinder kinetic energy from transferring to large scales, we consider a hyper-viscosity term $(+\nu_u \nabla^2 \bar{S}_{ij})$ as suggested by previous researchers.[4,13]

The mixed gradient-type consistent DSM (MGCDSM) is defined as

$$\tau_{ij} \approx \left(\frac{G_{ij}}{G_{mm}}\right) 2k_{\text{sgs}} + \nu_u \nabla^2 \bar{S}_{ij}\,, \quad \text{where } G_{ij} = \frac{\partial \bar{u}_i}{\partial x_k}\frac{\partial \bar{u}_j}{\partial x_k}\,. \tag{3}$$

Here, the hyper-viscosity magnitude ν_u can be calculated by either $\nu_u = C_s' \Delta^4 |\bar{S}|$ or $\nu_u = C_k' \Delta^3 \sqrt{k_{\text{sgs}}}$. Note that C_s' and C_k' can be determined by dynamic procedures. In this paper, we use the second method with an empirical constant $C_k' = 0.008$.

A second model can be formed using the fact that $L_{ij}^M + C_{ij}^M$ is MFI consistent. The mixed similarity-type consistent DSM (MSCDSM) is expressed as

$$\tau_{ij} \approx \left(\frac{\Upsilon_{ij}}{\Upsilon_{mm}}\right) 2k_{\text{sgs}} + \nu_u \nabla^2 \bar{S}_{ij}\,, \tag{4}$$

where $\Upsilon_{ij} = C_L L_{ij}^M + C_C[(\overline{\bar{\bar{u}}_i \bar{u}_j} - \bar{\bar{\bar{u}}}_i \bar{\bar{u}}_j) + (\overline{\bar{u}_i \bar{\bar{u}}_j} - \bar{\bar{u}}_i \bar{\bar{\bar{u}}}_j) - 2(\overline{\bar{\bar{u}}_i \bar{\bar{u}}_j} - \bar{\bar{\bar{u}}}_i \bar{\bar{\bar{u}}}_j)]$ is one possible model of $L_{ij}^M + C_{ij}^M$. When the cross term is approximated in the form of the generalized scale similarity model, C_C is a O(1) dimensionless coefficient,[17] and we adopt $C_C = 1.5$ in this paper.

2.3. *Numerical setup*

Direct numerical simulations and large eddy simulations have been performed using a pseudo-spectral code, which is similar to codes used in several previous studies.[29,37] In these codes, the linear viscosity and Coriolis terms are included with an integrating factor, which is helpful to increase numerical stability and to decrease numerical diffusion. In this study, the time advance is carried out through the use of an explicit third-order Runge–Kutta scheme, which is applied to the nonlinear term and the modeled SGS stress term. Note that direct numerical simulations exclude

the modeled SGS stress term. The highest available wave number is set according to the 2/3 de-aliasing rule.[8]

Decaying turbulent cases does not include any kinetic energy source. Forced turbulent cases use Gaussian white-noise forcing as an energy source, with forcing spectrum chosen to be Gaussian, $F(k) = \varepsilon_f \frac{\exp(-0.5(k-k_f)^2/\sigma^2)}{(2\pi)^{1/2}\sigma}$, where k_f is the forcing peak wave number. As a typical setup,[37] the standard deviation is taken to be $\sigma = 1$, and the energy input rate is approximately $\varepsilon_f = 1$.

The Rossby number characterizes the dimensionless ratio of the rotation time-scale $((2\Omega)^{-1})$ to a nonlinear time-scale. A micro-scale Rossby number Ro^{ω_3} is defined as $Ro^{\omega_3} = \omega_3'/(2\Omega)$, where ω_3' is the root-mean-square vorticity in the z-direction. When the Rossby number is large, the effects of rotation can be neglected. A small Rossby number indicates that the effects of rotation are comparably large. There are several challenges for LES of rapidly rotating flow with Rossby numbers less than unity. Accurate computations will reproduce at least four important features (some more prominent in forced flow as compared with decaying turbulence):

(i) significant net transfer of energy from small to large-scales;
(ii) scaling of the large-scale energy spectrum approximately $E(k) \approx E(k_h = \sqrt{k_x^2 + k_y^2}; k_z = 0) \propto k^{-3}$;
(iii) the generation of large-scale vortical columns, with dominance of cyclones over anti-cyclones; and
(iv) a tendency toward 2D and two-component flow, with much lower levels of energy in the velocity component parallel to the rotation axis.

Studies[7,36] have suggested that numerical simulations are restricted by resolution constraints to moderately small Rossby numbers less than unity. With guidance from previous studies,[3,5] we have performed simulations over a range of $0.1 \lesssim Ro^{\omega_3} \lesssim 0.4$.

We solve the LES equations (1) numerically on a mesh of spacing $h = 2\pi/\max(nx, ny, nz)$, where nx, ny, and nz are the point numbers in the x-, y-, and z-directions, and treat $\Delta = 2h$ for sixth-order accuracy.[40,9] For simplicity, we use some abbreviated expressions below: "large eddy simulation using SM" is abbreviated as "SM," "large eddy simulation using SM at the resolution of 32^3" is abbreviated as "32^3 SM," etc.

3. Decaying Turbulence

Decaying rotating turbulence, which ignores the effects of forcing, is a typical setup for the assessment of SGS models. In this section, we apply models to an isotropic turbulent decaying case and a rotating turbulent decaying case. The initial Taylor micro-scale Reynolds number (Re_λ) is about 85. Thus, the 128^3 DNS has resolved flow of all scales, and the DNS results can be used to verify the accuracy of SGS models and identify their problems. We set a rather restrictive Courant–Friedrichs–Lewy number of ~ 0.15 for decaying simulations.
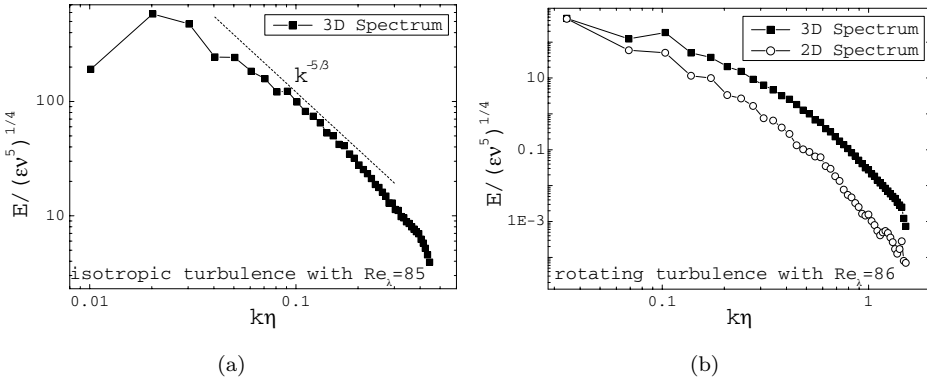
Fig. 1.   Normalized kinetic energy spectra of DNS cases in their initial stages: (a) 3D kinetic energy spectrum of Case A; (b) 3D and 2D kinetic energy spectra of Case B.

Case A starts from an isotropic turbulent state derived from an isotropic case, which has been described extensively in a previous article.[25] After that case has reached its statistically steady state, we turn off the forcing. The flow decays over about two initial eddy turn-over times and reaches the initial state for isotropic Case A, which has $Re_\lambda = 85$. The eddy turn-over time is defined as $\tau = K/\varepsilon$, where K is the total kinetic energy and ε is the total dissipation rate. Figure 1(a) shows the normalized 3D kinetic energy spectrum $(E(k)/(\varepsilon\nu^5)^{1/4})$ of this initial state; to compare with the Kolmogorov spectrum, a $-5/3$ power law is shown as a dotted line.

Case B starts from a rotating turbulent state. We use the Gaussian forcing to add energy at large scales ($k_f = 2.5$) to an initial very low energy isotropic random noise, and add rotational force from the very beginning. Such a problem has been studied extensively in the past.[37,36] Then, we stop the forced run at a statistically steady state to provide the initial state for Case B, which has $Re_\lambda = 86$ and $Ro^{\omega 3} = 0.41$ ($\Omega = 1$). Figure 1(b) shows the normalized 3D kinetic energy spectrum and the normalized 2D kinetic energy spectrum $(E(k_h; k_z = 0)/(\varepsilon\nu^5)^{1/4})$ of this initial state.

At the *a posteriori* test level, the "grid" level filter shape is not explicitly specified. We assume the Gaussian filtering at the "grid" level in order to obtain the filtered DNS results. Note that we have filtered DNS data (including initial conditions) with cutoff wave number, $k_c = 21$, to derive the 64^3 LES field and with $k_c = 11$ to derive the 32^3 LES field. We have normalized time using initial eddy turn-over time for subsequent discussions.

3.1. *Results and discussions*

Figures 2 and 3 show the evolution of the total resolved kinetic energy, $K_r = \int (1/2)\bar{u}_i\bar{u}_i d\mathbf{x}$. Clearly, the simulation without a model yields the worst prediction
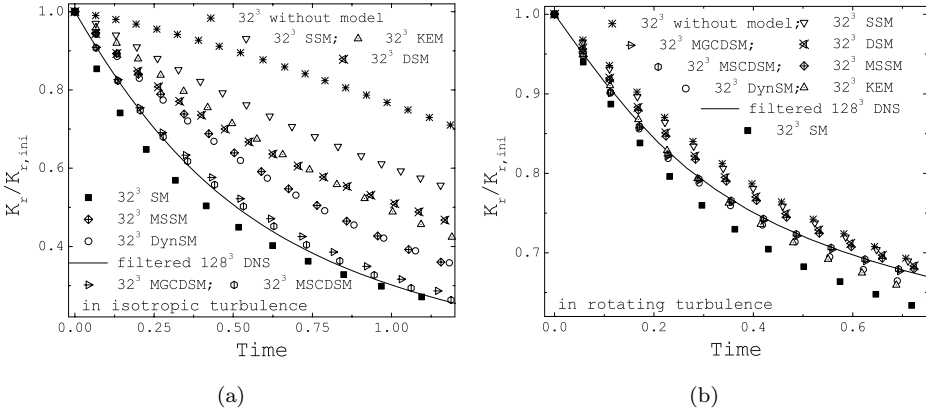
Fig. 2. Total resolved kinetic energy evolution obtained from the filtered 128^3 DNS, and various 32^3 large eddy simulations in (a) Case A and (b) Case B.
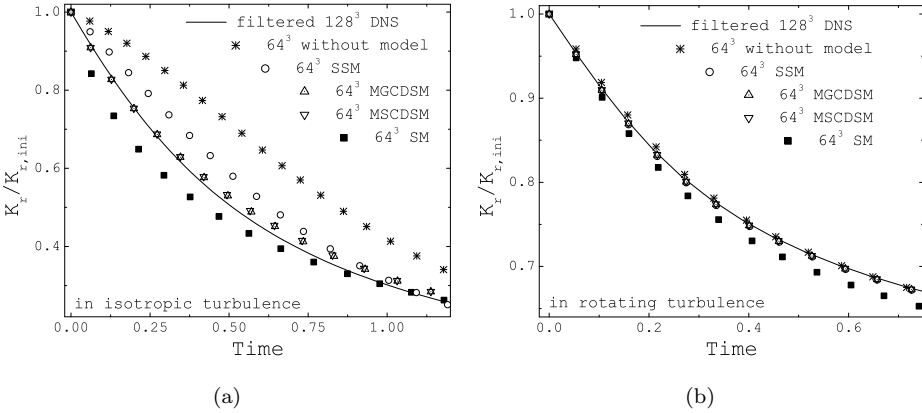

Fig. 3. Total resolved kinetic energy evolution obtained from the filtered 128^3 DNS and various 64^3 large eddy simulations in (a) Case A and (b) Case B.

and the results from two new models, the MGCDSM and the MSCDSM, are in excellent agreement with the filtered DNS results.

The simulation without a model simply omits τ_{ij}. The decaying cases start at the initial Reynolds number of about 85 and are exceedingly beyond the capability of 32^3 simulation (typically $\mathrm{Re}_\lambda \sim 30$). Thus, the total resolved kinetic energy obtained from the 32^3 simulation without a model decreases more slowly. Figure 4 illustrates that kinetic energy at small scales is hardly dissipated. Together with the fact that a great amount of kinetic energy at large scales transfers into small scales,[26] turbulent flow is accumulating kinetic energy at small scales. The increase of grid resolution from 32^3 (Fig. 2) to 64^3 (Fig. 3) facilitates the prediction of the kinetic energy decay. However, in Case A, the 64^3 simulation without a model still

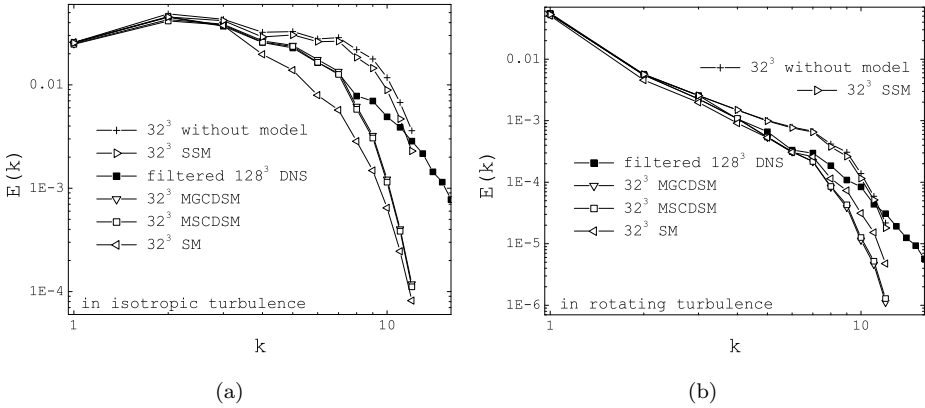(a)   (b)

Fig. 4.   3D kinetic energy spectrum obtained from the filtered 128^3 DNS, the 32^3 SM, the 32^3 SSM, the 32^3 MGCDSM, and the 32^3 MSCDSM in (a) Case A at time = 0.4 and (b) Case B at time = 0.7.

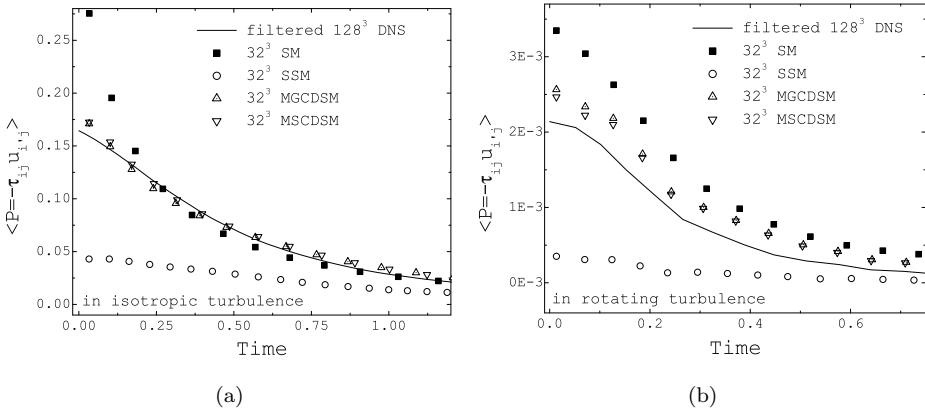(a)   (b)

Fig. 5.   SGS energy production evolution obtained from the filtered 128^3 DNS, the 32^3 SM, the 32^3 SSM, the 32^3 MGCDSM, and the 32^3 MSCDSM in (a) Case A and (b) Case B.

yields a much lower kinetic energy decay rate. In order to obtain proper kinetic energy decay rates, turbulence modeling is needed for coarser grids.

The decay of the total resolved kinetic energy is described by $(DK_r/Dt) = -\int P d\mathbf{x} - \int \varepsilon_r d\mathbf{x}$, where $\varepsilon_r = \nu(\partial \bar{u}_i/\partial x_j)(\partial \bar{u}_i/\partial x_j)$ is the molecular dissipation, and $P = -\tau_{ij}(\partial \bar{u}_i/\partial x_j)$ is the SGS energy production (sometimes referred to as "energy flux"). The SGS energy production represents the kinetic energy transfer from resolved scales to SGS and is regarded as the kinetic energy source at SGS. The rotational term will not explicitly appear in this equation, since analytically $(\mathbf{\Omega} \times \bar{\mathbf{u}}) \cdot \bar{\mathbf{u}} = 0$. Figure 5 shows the SGS energy production evolution. The simulation without a model has no SGS energy production, since no SGS model is adopted. Figure 6 shows the evolution of the normalized (by initial value) molecular dissipation.
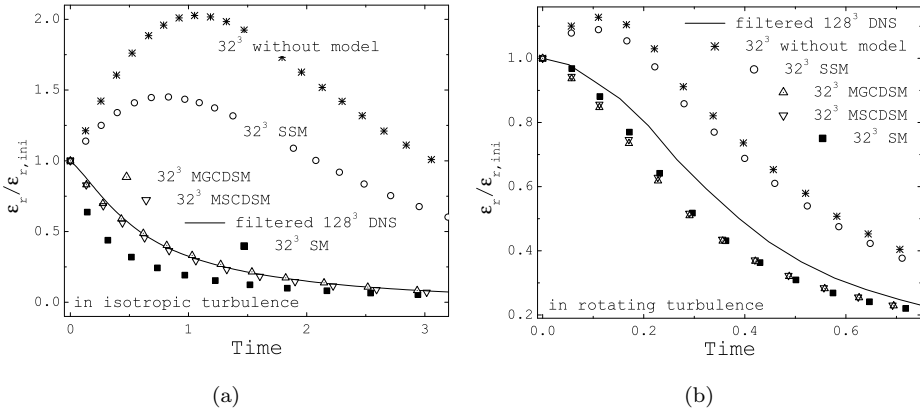
Fig. 6. Molecular dissipation evolution obtained from the filtered 128^3 DNS, the 32^3 SM, the 32^3 SSM, the 32^3 MGCDSM, and the 32^3 MSCDSM in (a) Case A and (b) Case B.

Figures 2 and 3 show that the SM yields higher kinetic energy decay rates in comparison with the filtered DNS results. Figure 4 shows that kinetic energy over a wide range of length scales is dissipated excessively in simulations using the SM. In principle, SGS models represent the effects of the unresolved SGS motions on the resolved scales, and the large-scale flows are solved explicitly. Thus, the excessive dissipation at large scales may be considered as an incorrect manner. Further, Fig. 5 shows that the SM yields higher SGS energy production over a long period of time, and this indicates that too much kinetic energy has been delivered to SGS.

The SSM resolves many weaknesses of the SM: for instance, it allows for "backscatter" and yields high correlations ($\rho > 0.6$) with the SGS stress over a wide range of filter sizes.[24,25] Figure 2 shows that, over a long period of time, the SSM yields lower kinetic energy decay rates in both Cases A and B. It is consistent with previous findings that the SSM is not dissipative.[1] In Case B, the SSM performs as poorly as the simulation without a model. Kinetic energy at small scales is accumulating and cannot be dissipated effectively, as shown in Fig. 4. The primary reason is that the SSM yields much lower SGS energy production (Fig. 5); thus, there is an insufficient transfer of kinetic energy to SGS using the SSM. Figure 6 shows that the presence of too many small scales leads to the over-predicted molecular dissipation for both the 32^3 simulation without a model and the SSM. In this manner, the molecular dissipation takes over part of the work that the SGS energy production should have performed. Further, if the grid resolution is increased from 32^3 (Fig. 2) to 64^3 (Fig. 3), the SSM delivers much better results. This strong resolution dependence implies the possibility that a model could yield significantly different global results for different resolutions and may be considered as a crucial disadvantage of the SSM.

The DynSM, the MSSM, the KEM, and the DSM are developed to resolve disadvantages of earlier models. Figure 2 has shown that they can deliver more

accurate kinetic energy decay rates than the SSM. In Case A, the DynSM and the MSSM yield better outcomes of kinetic energy; however, four models still fail to yield sufficient dissipation and result in lower kinetic energy decay rates. In Case B, over all the DynSM and the KEM yield better outcomes of kinetic energy, and the MSSM yields slightly better results than the SSM. The expressions of the DynSM, the KEM, and the MSSM include eddy viscosity terms; however, the DSM is a one-equation nonviscosity model. Pomraning and Rutland[33] found that the DSM yields good results in low Reynolds number isotropic flows. In both high-Reynolds number cases A and B, the DSM is also capable of providing dissipation (but insufficiently) and initially yields results similar to those of the other three models.

As shown in Figs. 2 and 3, the total resolved kinetic energy results obtained from the new models are in excellent agreement with the filtered DNS data, and the results are also very consistent across different resolutions. In Case A, the new models yield accurate SGS energy production [Fig. 5(a)] and accurate molecular dissipation [Fig. 6(a)]. In Case B, they yield slightly lower levels of molecular dissipation [Fig. 6(b)]; however, they compensate this somewhat minor weakness by slightly over-predicting SGS energy production, as shown in Fig. 5(b).

Figure 7 compares the SM (as a representative of eddy viscosity closure) and the MGCDSM with respect to a $\partial \tau_{ij}/\partial x_j$ power spectrum, which is normalized by a magnitude at $k = 21$. The influences of the MGCDSM on large-scale flows are comparably minor, and the SM yields more dissipation over all scales. Energy spectrum comparisons (Fig. 4) have demonstrated that the new models yield more accurate results at large scales than the SM.

Using a one-equation approach enables us to calculate the ratio of SGS kinetic energy $(K_{\text{sgs}} = \int (1/2)\tau_{ii} d\mathbf{x})$ to total kinetic energy $(K_{\text{sgs}} + K_r)$, and this calculation describes the dominant level of SGS to resolved scales. The SGS flows,
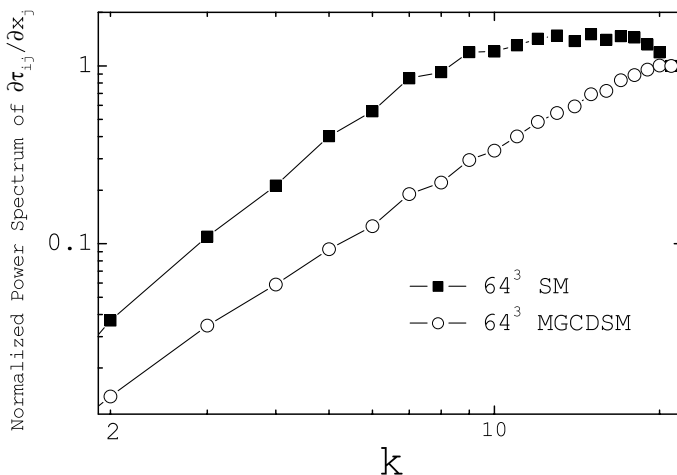

Fig. 7.   Normalized (at $k = 21$) power spectrum of $\partial \tau_{ij}/\partial x_j$ obtained from the 64^3 SM and the 64^3 MGCDSM in the LES of Case A.

which initially account for $\sim 35\%$ ($\sim 16\%$) of the turbulent kinetic energy at the resolution of 32^3 (64^3), are of great intensity for current cases, and thus the imperfect modeling of SGS stress may cause significant disagreement with the filtered DNS results. It has been illustrated that at the *a priori* test level, the MFI consistent DSMs are more accurate in both isotropic turbulence and rotating turbulence.[25] This fact offers another reason why the new models yield more accurate *a posteriori* results.

4. Forced Rotating Turbulence

Unlike many previous studies, such as rotating turbulence in channel,[12,31] which involves certain kinetic energy sources, in this section we assess models by including Gaussian forcing in rotating turbulence, excluding boundary layer effects. The large eddy simulations are forced either at large scales ($k_f = 2.5$) or at intermediate scales ($k_f = 12$). The molecular viscosity, hypo-, and hyper-viscosities have been turned off, thus, the modeled SGS stress plays an important role in kinetic energy transfer. All eight SGS models have been assessed using the same numerical setup and all simulations have reached their statistically steady states. Corresponding (match Ro^{ω_3}) benchmark simulations have been performed at the resolution of 128^3. Among the traditional models, the SM is the most used SGS model in engineering applications, and the MSSM has the most superior performance. Note that in forced testing, the performances of the two new models are very similar to each other; thus, the results obtained from the MSCDSM are excluded.

Figure 8(a) shows the 3D and 2D kinetic energy spectra in a statistically steady state obtained from the 64^3 MGCDSM. The history of the resolved kinetic energy is also included to demonstrate one example of all simulations, which have reached their statistically steady states, and we normalize time using $T = 2\pi/\Omega$. The flow

<div align="center">(a)</div>
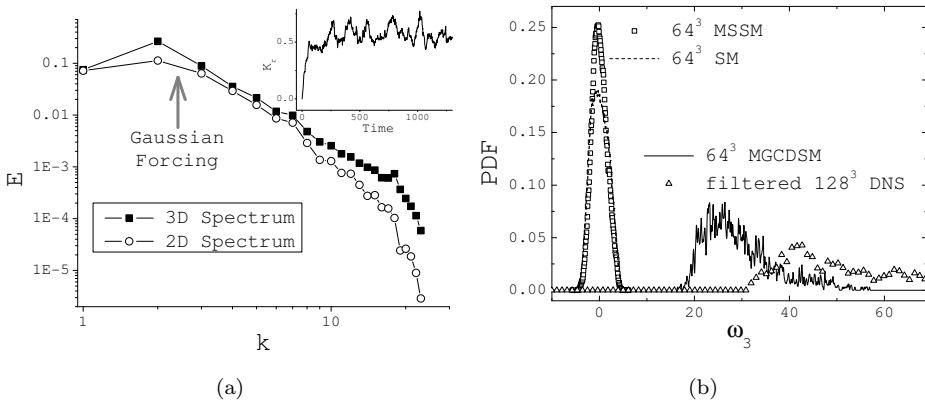<div align="center">(b)</div>

Fig. 8.   Assessment of the 64^3 LES of large-scale forced rotating turbulence at statistically steady state: (a) 3D and 2D kinetic energy spectra (obtained from the 64^3 MGCDSM), including the history of resolved kinetic energy K_r; (b) PDF of ω_3 obtained from the filtered 128^3 DNS, the 64^3 SM, the 64^3 MSSM, and the 64^3 MGCDSM.

is forced at large scales, and we use a constant $\Omega = 12$ to achieve $Ro^{\omega_3} = 0.12$. The MGCDSM facilitates the two-dimensionalization process resulting in very close 3D and 2D energy spectra at large scales, $k \lesssim 7$. Except for the MGCDSM and the MSCDSM, all other examined models fail to deliver this quasi-2D structure at large scales.

In order to examine the cyclonic/anti-cyclonic asymmetry, we concentrate on vortex regions rather than the whole domain, in which small ω_3 vortices are still dominating.[30] The vortex regions can be identified using the criterion $\lambda_2 < 0$[a] for a vortex region,[19] and we sample over points with $\lambda_2 < (1/6) \min(\lambda_2) < 0$ to obtain the $PDF(\omega_3)$. Figure 8(b) compares the SM, the MSSM, and the MGCDSM with respect to the $PDF(\omega_3)$. The MGCDSM successfully delivers the cyclonic/anti-cyclonic asymmetry (the dominance of positive ω_3 vortices); others fail to do so.

Figure 9 examines the MGCDSM at the resolution of 32^3. The Rossby number of the statistically steady state is $Ro^{\omega_3} = 0.1$ ($\Omega = 2$). Comparing the kinetic energy spectrum plots of Figs. 8(a) and 9(a), even though the model performs worse at this coarser grid, it is still able to deliver the cyclonic/anti-cyclonic asymmetry.

Figure 10 examines the 64^3 intermediate-scale forced large eddy simulations. In the simulation using the MGCDSM, we use a constant $\Omega = 8$ to achieve $Ro^{\omega_3} = 0.16$. As shown in Fig. 10(a), the MGCDSM yields sufficient dissipation of kinetic energy at small scales and captures the reverse energy transfer to large scales. Figure 10(b) compares SGS models with respect to $PDF(\omega_3)$ and shows that the MGCDSM is able to deliver the cyclonic/anti-cyclonic asymmetry.
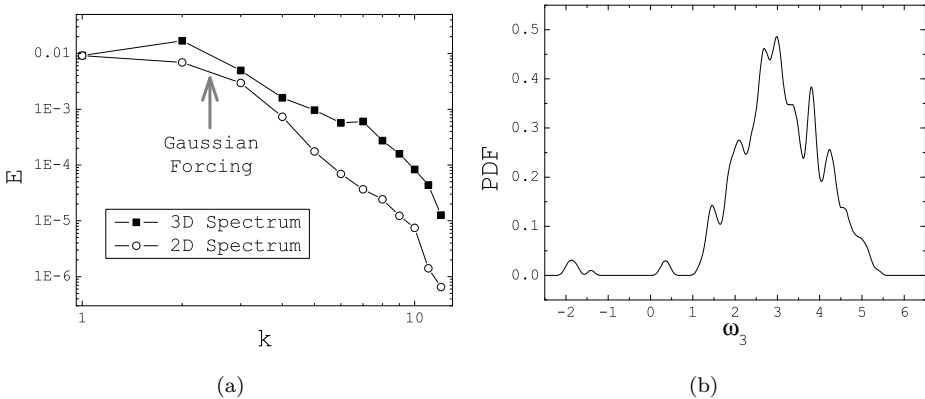

(a)

(b)

Fig. 9.   Assessment of the 32^3 LES of large-scale forced rotating turbulence using the MGCDSM at statistically steady state: (a) 3D and 2D kinetic energy spectra; and (b) PDF of ω_3.

[a]λ_2 is the second large eigenvalue of tensor $S_{im}S_{mj} + \Omega_{im}\Omega_{mj}$, where $\Omega_{ij} = (1/2)(\partial u_i/\partial x_j - \partial u_j/\partial x_i)$.
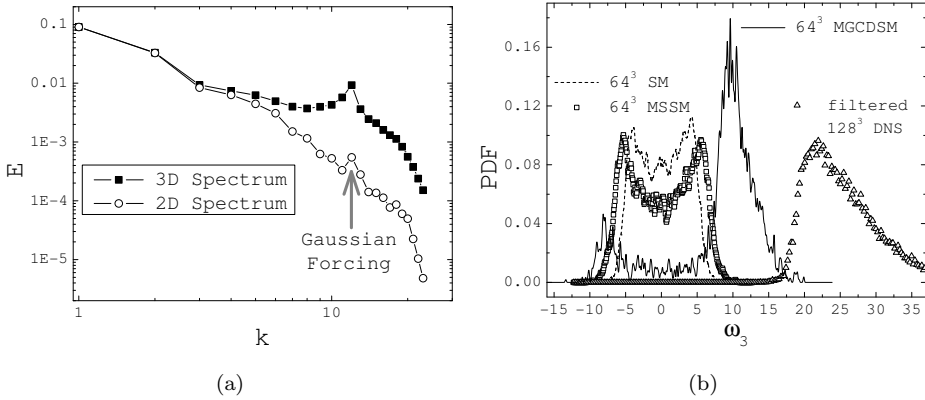
(a)   (b)

Fig. 10. Assessment of the 64^3 LES of intermediate-scale forced rotating turbulence at statistically steady state: (a) 3D and 2D kinetic energy spectra (obtained from the 64^3 MGCDSM); (b) PDF of ω_3 obtained from the filtered 128^3 DNS, the 64^3 SM, the 64^3 MSSM, and the 64^3 MGCDSM.

5. Summary and Conclusion

We have presented the *a posteriori* testing results of various SGS models. The SM, the SSM, and the KEM are the basis for the latter models. Two flow configurations (i.e., decaying turbulence and forced rotating turbulence) have been used. The LES results in the first configuration have been compared with DNS data, and in the analysis of forced rotating turbulence we substantially focus on the anisotropic features of rotating turbulence.

In the first series of simulations, the quality of a model is determined by the discrepancy of its results with the filtered DNS results. In order to determine whether the model is helpful, comparisons with a coarse grid simulation without a model have been performed. Table 1 summarizes the results. The models are listed with symbols to indicate if they performed poorly or well on each diagnostic. If we arrange the models with respect to the overall accuracy (from higher to lower) of their results, we may roughly obtain the following sequence: MSCDSM (and MGCDSM), MSSM (DynSM and KEM), DSM (SM and SSM).

Table 1. Comparison of model performance in the LES of decaying turbulence (initially with high Reynolds number) at the *a-posteriori* test level.

Diagnostic	SM	KEM	DynSM	SSM	MSSM	DSM	MSCDSM	MGCDSM
Kinetic energy	−	0	0	−	−	−	+	+
SGS production	−	0	0	−	−	−	+	+
Dissipation	0	0	0	−	−	−	+	+
Energy spectrum	−	+	+	−	+	−	+	+

The symbols − and + refer to bad and good results. The symbol 0 refers to bad results in isotropic case, but good results in rotating turbulent case.

DSMs are one class of one-equation models. Differing from zero-equation models (e.g., SM and DynSM), one-equation models do not assume the local balance between the SGS kinetic energy production and dissipation rate; thus, they do not require *a priori* knowledge to set model constants (e.g., C_s). Moreover, studies have shown that at the *a priori* test level, one-equation models improve the accuracy of SGS stress modeling,[27,25] and for rotating turbulence, the MFI consistent DSMs deliver more accurate modeling of SGS stress in all directions.[25]

The overall results indicate that mixed models can yield better performance. This fact has also been observed in many previous studies.[42,40] The additional eddy viscosity term is usually much smaller ($\lesssim 50$ times when measured in the L_2-norm) than the original structure term; thus, it does not degrade the *a priori* results.[24,25] An analytical point of view is that the eddy viscosity term is modeling of the higher-order term of the Taylor expansion of SGS stress or the modified SGS Reynolds stress term. The eddy viscosity term is trace free. Thus, it does not change the trace of the original structure term, and mixed DSMs still satisfy the trace requirement $\tau_{ii}^{\mathrm{model}} = \tau_{ii}$. More importantly at the *a posteriori* test level, the eddy viscosity term significantly facilitates the kinetic energy dissipation at small scales and stabilizes the simulation.[1,42,40] The original model usually fails to perform so.

The eddy viscosity term transfers kinetic energy only from resolved scales to SGS. As is well known, the SM yields excessive dissipation in low-Reynolds number isotropic turbulence,[10] turbulent channel flow,[32] turbulent mixing layer,[40] and many other flows. Note that the SM is excessively dissipative over a wide range of length scales, and this behavior certainly affects the large-scale flow structure in rotating turbulence. Two later models, the DynSM and the KEM, are slightly over dissipative; however, they yield much more accurate results in high-Reynolds number rotating turbulence.

Examination of the kinetic energy spectrum demonstrates that the MGCDSM and the MSCDSM deliver more accurate amounts of large scales and sufficient dissipation at small scales. During to insufficient dissipation at small scales by SGS models, the high-Reynolds number flow simulated using the SSM, the MSSM, the DSM, the KEM (does not apply to rotating turbulence), and the DynSM (does not apply to rotating turbulence) contains too much small-scale energy. This yields a higher molecular dissipation, which supplements the insufficient small-scale dissipation. Note that in rotating turbulence the KEM and the DynSM yield good agreement with the filtered DNS results.

The second series of simulations concerns rotating turbulence at a much higher Reynolds number, and we focus the assessment of SGS models on the capability of capturing essential characteristic features of rotating turbulence. Table 2 summarizes the results.

Although the SM and the MSSM carry eddy viscosities, they are not MFI consistent,[25] and may have disadvantages. Specifically, in large-scale forced rotating turbulence, kinetic energy at large scales is dissipated excessively in simulations

Table 2. Comparison of model performance in the LES of forced rotating turbulence at the *a posteriori* test level.

Diagnostic	SM*	SSM	MSSM	DSM	MGCDSM	MSCDSM
Cyclonic/anticyclonic asymmetry	−	−	−	−	+	+
Quasi-2D flow at large scales	−	−	−	−	+	+
Reverse energy transfer**	+	−	+	−	+	+

The symbols − and + refer to bad and good results. *: including the KEM and the DynSM. **: only in intermediate-scale forced rotating turbulence.

using the SM. In intermediate-scale forced rotating turbulence, they yield sufficient dissipate of kinetic energy at small scales and are capable of delivering kinetic energy from small to large scales. However, most importantly, they fail to deliver the cyclonic/anti-cyclonic asymmetry.

Comparing with traditional models, the MGCDSM and the MSCDSM are better able to capture essential features of rotating turbulence. They not only adequately suppress the small-scale flows, but also facilitate the kinetic energy transfer from small to large scales and generate more accurate large-scale flows, including quasi-2D and cyclonic structures.

Despite offering a large improvement, the results obtained using the new models still show discrepancies in some aspects. Additional improvement of LES modeling may be guided by the present results. Moreover, there exists a need to study more complex flows (e.g., rotating stratified turbulence and channel flow subject to system rotation), which are physically realizable and admit a quantitative comparison with experimental results.

Acknowledgments

References

1. J. Bardina, J. H. Ferziger and W. C. Reynolds, *AIAA Paper 80-1357* (1980).
2. C. N. Baroud, B. B. Plapp, H. L. Swinney and Z.-S. She, *Phys. Fluids* **15**, 2091 (2003).
3. P. Bartello, O. Metais and M. Lesieur, *J. Fluid Mech.* **273**, 1 (1994).
4. C. Basdevant and R. Sadourny, *J. Méc. Théor. Appl., Numéro Spéc.* 243 (1983).
5. L. Bourouiba and P. Bartello, *J. Fluid Mech.* **587**, 139 (2007).
6. J. Boussinesq, *Acad. Sci. Inst. Fr., Paris* **23**, 46 (1877).
7. C. Cambon, N. N. Mansour and F. S. Godeferd, *J. Fluid Mech.* **337**, 303 (1997).
8. C. Canuto, M. Y. Hussaini, A. Quarteroni and T. A. Zang, *Spectral Methods in Fluid Dynamics* (Sprnger-Verlag, Berlin Heidelberg, 1988).

9. F. K. Chow and P. Moin, *J. Comput. Phys.* **184**, 366 (2003).
10. S. G. Chumakov and C. J. Rutland, *Int. J. Numer. Meth. Fluids* **47**, 911 (2005).
11. R. A. Clark, J. H. Ferziger and W. C. Reynolds, *J. Fluid Mech.* **91**, 1 (1979).
12. J. W. Deardorff, *J. Fluid Eng.* **95**, 429 (1973).
13. J. H. Ferziger, *Large Eddy Simulation — A Short Course* (Stanford University, 2000).
14. C. Fureby and G. Tabor, *Theor. Comput. Fluid Dyn.* **9**, 85 (1997).
15. M. Germano, U. Piomelli and W. H. Cabot, *Phys. Fluids A* **3**, 1760 (1991).
16. S. Ghosal, T. S. Lund, P. Moin and K. Akselvoll, *J. Fluid Mech.* **286**, 229 (1995).
17. K. Horiuti, *Phys. Fluids* **9**, 3443 (1997).
18. K. Horiuti, *J. Turbulence* **7**, 1 (2006).
19. J. Jeong and F. Hussain, *J. Fluid Mech.* **285**, 69 (1995).
20. W.-W. Kim and S. Menon, *AIAA Paper 1995-356* (1995).
21. H. Kobayashi and Y. Shimomura, *Phys. Fluids* **13**, 2350 (2001).
22. D. K. Lilly, *Proc. IBM Scientific Computing on Symposium on Environmental Sciences* (Yorktown Heights, New York, 1967), p. 167.
23. D. K. Lilly, *Phys. Fluids* **4**, 633 (1992).
24. S. Liu, C. Meneveau and J. Katz, *J. Fluid Mech.* **275**, 83 (1994).
25. H. Lu, C. J. Rutland and L. M. Smith, *J. Turbulence* **8**, 1 (2007).
26. J. L. Lumley, *Phys. Fluids A* **4**, 203 (1992).
27. S. Menon, P.-K. Yeung and W.-W. Kim, *Comput. Fluids* **25**, 165 (1996).
28. Y. Morinishi, K. Nakabayashi and S. Q. Ren, *Phys. Fluids* **13**, 2912 (2001).
29. Y. Morinishi, K. Nakabayashi and S. Q. Ren, *Int. J. Heat Fluid Flow* **22**, 30 (2001).
30. C. Morize, F. Moisy and M. Rabaud, *Phys. Fluids* **17**, 1 (2005).
31. U. Piomelli and J. Liu, *Phys. Fluids* **7**, 839 (1995).
32. U. Piomelli, T. A. Zang, C. G. Speziale and M. Y. Hussaini, *Phys. Fluids A* **2**, 257 (1990).
33. E. Pomraning and C. J. Rutland, *AIAA J.* **40**, 689 (2002).
34. Y. Shimomura, *J. Phys. Soc. Jpn.* **68**, 2483 (1999).
35. J. Smagorinsky, *Mon. Weather Rev.* **91**, 99 (1963).
36. L. M. Smith and Y. Lee, *J. Fluid Mech.* **535**, 111 (2005).
37. L. M. Smith and F. Waleffe, *Phys. Fluids* **11**, 1608 (1999).
38. C. G. Speziale, *Geophys. Astrophys. Fluid Dynam.* **33**, 199 (1985).
39. B. Vreman, B. Geurts and H. Kuerten, *Phys. Fluids* **6**, 4057 (1994).
40. B. Vreman, B. Geurts and H. Kuerten, *J. Fluid Mech.* **339**, 357 (1997).
41. A. Yoshizawa and K. Horiuti, *J. Phys. Soc. Jpn.* **54**, 2834 (1985).
42. Y. Zang, R. L. Street and J. R. Koseff, *Phys. Fluids A* **5**, 3186 (1993).